Vibrational Relaxation of Matrix-Isolated Carboxylic Acid Dimers and Monomers[†]

Ermelinda M. S. Maçôas,*[,‡,§] Pasi Myllyperkiö,[‡] Henrik Kunttu,[‡] and Mika Pettersson[‡]

Nanoscience Center, Department of Chemistry, P.O. Box 35, University of Jyväskylä, FI-40014 Finland

Received: November 11, 2008; Revised Manuscript Received: February 10, 2009

Femtosecond mid-IR transient absorption spectroscopy was used to probe the vibrational dynamics of formic acid and acetic acid isolated in solid argon following excitation of the fundamental transition of the carbonyl stretching mode. Carboxylic acids form extremely stable H-bonded dimers, hindering the study of the monomeric species at equilibrium conditions. The low-temperature rare-gas matrix isolation technique allows for a unique control over aggregation enabling the study of the monomer vibrational dynamics, as well as the dynamics of two distinct dimer structures (cyclic and open chain). This study provides insight into the role of the methyl rotor and hydrogen bonding in the vibrational dynamics of carboxylic acids. In the monomer of FA, depopulation of the initially excited state is characterized by a time constant of approximately 500 ps, and it is followed by the energy transfer from intermediately populated intramolecular vibrational states into the phonon modes of the argon lattice (vibrational cooling) in a much longer time scale (estimated to be longer than 5 ns). The methyl rotor in acetic acid monomer accelerates both processes of population transfer and vibrational cooling, with time constants of ~80 ps. Hydrogen bonding in formic acid dimers decreases the time constant associated with the dominant vibrational relaxation process by more than 2 orders of magnitude. Unlike in formic acid, hydrogen bonding in acetic acid has no apparent effect on the vibrational cooling rate.

Introduction

Monocarboxylic acids exhibit various fascinating properties that have made them the focus of a vast body of experimental and theoretical studies. They have been used as prototype systems to understand IR-induced isomerization,[1−3] proton tunneling in a bound asymmetric potential,[4,5] intermolecular hydrogen bonding,[6−8] and double proton transfer.[9−12] However, investigation of the monomer species in the condensed phase has been hampered by the difficulties in preparing samples with high monomer content. For formic acid (FA) and acetic acid (AA), the lowest energy dimer is estimated to be about 12−16 kcal/mol more stable than the isolated monomers.[7,13,14] Monomers of carboxylic acids can conveniently be studied in low temperature matrix isolation conditions, where the dimer to monomer ratio can be controlled by changing the sample preparation parameters.[7,15] A matrix where the monomer concentration exceeds that of the dimer by 1 order of magnitude can be prepared by continuous flow deposition of a diluted gaseous mixture (1/1000 for FA(AA)/rare gas).[16,17] Pulse deposition techniques were also shown to be very efficient in controlling the monomer/dimer ratio by tuning the gas pulse duration.[7,15]

Even though the dynamics of vibrational relaxation of the monomer have not been directly studied, many processes intimately connected with the vibrational energy redistribution and relaxation phenomena in the monomer have been investigated. Observation of IR-induced conformational isomerization in monomeric FA isolated in rare-gas matrices has inspired many studies including conformationally selective UV-photolysis,[18] IR-induced isomerization below the C−O torsional barrier, and phonon-assisted tunneling of the high energy conformer (cis-form, −COOH dihedral angle of 0°) to the conformational ground state (trans-form, −RCOH dihedral angle of 180°).[1,5] More recently, IR-induced trans → cis isomerization has also been investigated in the open-chain dimer.[19] Additionally, due to the low energy barrier (2 kcal/mol), the open-chain dimer can be thermally converted into the most stable cyclic dimer in low temperature matrices by rotation around the C═O···HO intermolecular bond.[7] H-bonding was shown to have an important role in quenching tunneling of the free hydrogen in formic acid dimers and in its water complex, thus stabilizing the high energy form.[4,6]

As far as we know, the only time-resolved studies that include both monomers and dimers of carboxylic acid have used femtosecond degenerate four wave mixing, in the gas cell at room temperature and under supersonic jet conditions (60−90 K), to obtain the rotational and centrifugal distortion constants, and the parametrized polarizability.[20,21] No information on the vibrational dynamics was derived from those studies. Contrary to the monomer, dimers of small monocarboxylic acids, in particular the most stable 8-membered-ring centrosymmetric dimer of FA and AA, have been extensively studied by time-resolved IR-spectroscopy, both in the gas phase and in solution. Most of the studies have followed the dynamics upon excitation of the fundamental transitions of the OH,[22−28] CH, and C═O,[29−31] stretching modes yielding information on the mechanisms of energy relaxation, such as the importance of the anharmonic couplings to low frequency intermolecular modes. A common feature in the vibrational dynamics upon excitation of the OH stretching fundamental (ν_{OH}) in monocarboxylic acid dimers in solution is a biexponential vibrational energy redistribution kinetics with a faster subpicosecond component due to local energy redistribution to states that are strongly coupled to the excited mode, and a slower (1−4 ps) redistribution to the bath of intramolecular modes. Thermalization of the

[†] Part of the "Robert Benny Gerber Festschrift".

* Corresponding author. E-mail: emacoas@qui.uc.pt.

[‡] University of Jyväskylä.

[§] Current address: Department of Chemistry, University of Coimbra, P-3004-535 Coimbra, Portugal.

10.1021/jp8099384 CCC: $40.75
Published on Web 03/10/2009

system as the energy flows into the surrounding solvent takes place in a 10−20 ps time scale.[22,23,26,28,29] The similarities between the dynamics observed upon excitation of the ν_{OH} in the previously investigated carboxylic acids would suggest that the modes outside the ring are of less importance.

Excitation of the OH stretching leads to weakening of the hydrogen bond in solution and promotes ring opening and dissociation of the aggregates in the gas phase.[22,23] Probing the dynamics upon excitation at the fundamental transition of the C═O stretching ($\nu_{C=O}$) near 1770 cm^{-1} reduces effects due to isomerization and bond breaking. For the AA dimer in CCl_4 solution, the ground vibrational state of the $\nu_{C=O}$ shows a biexponential recovery upon excitation of the $\nu_{C=O}$ mode, with a dominant fast subpicosecond decay and a slow decay within 10 ps.[31] No bond breaking or bond weakening was reported. Methyl acetate was used as a prototype compound for monomeric AA exhibiting relaxation dynamics similar to that of the AA dimer, but with a dominant contribution arising from the slower decay pathway.[31] The fact that rotational diffusion, vibrational relaxation, and pure dephasing times were all shown to be comparable suggests that population relaxation was not dynamically averaged over all solvent configurations, and thus solvent memory effects could be at the origin of the observed nonexponential population relaxation.[31]

In this work, the aim is at investigating the relaxation dynamics of both monomers and dimers of FA and AA by combining ultrafast transient IR spectroscopy with rare-gas matrix isolation. Apart from allowing a unique control over aggregation, solid rare gases constitute a weakly interacting medium. To the best of our knowledge, only recently has a similar experimental approach been successfully applied to a series of studies of conformational isomerization in HONO.[32−34] Comparing the results reported here with the available data from solution studies provides information on the environmental effects on the relaxation dynamics of carboxylic acids.

Experimental Details

The gaseous samples were prepared by mixing FA (HCOOH, Riedel-Haen >98%) or AA (CH_3COOH, J. T. Baker >99%), degassed by several freeze−pump−thaw cycles, with high purity argon (AGA, 99.9999%), in proportions varied from 1.4% to 0.3%. Using FTIR spectroscopy (Nicolet Magna 760 spectrometer with KBr beamsplitter and nitrogen cooled MCT detector, 0.25 cm^{-1} resolution with 500 scans averaged), pulsed and continuous flow deposition techniques were carefully investigated to evaluate which technique would provide the most suitable matrices in terms of good transparency, acceptable matrix preparation times, and best control over the monomer to dimer ratio. Continuous deposition techniques proved to give better optical quality matrices (more transparent), while at the same time allowing for a good control over aggregation by choosing an appropriate concentration, matrix thickness, and deposition rate. Therefore, the matrix samples were prepared by continuous deposition of the gaseous mixtures onto a CaF_2 substrate kept at 15 K by a closed cycle helium cryostat (APD cryogenics). The deposition rate was typically 0.02 mmol/min. The deposition times varied between 30 to 70 min depending on the desired matrix thickness, which was kept below 20 μm. The matrix thickness can be determined from modulation observed in the IR spectrum caused by the interference of the transmitted beam with the beam reflected from the matrix interfaces.[35] Thicker and more concentrated samples favor the dimeric trapping of the guest (for FA, 1.4% mixture, ∼20 μm matrix), while the monomer/dimer ratio is increased in thinner and more diluted samples (for FA(AA), 0.4% (0.3%) mixture, ∼10 μm matrix).

The excitation and detection setup (mid-IR pump and mid-IR probe spectrometer) is based on a Ti:Sapphire oscillator (Coherent, Mira 900) and a multipass amplifier (Quantronics, Odin) providing 800 nm pulses of 100 fs duration and 0.8 mJ of energy operating at 1 kHz repetition rate. Tunable mid-IR pulses (3−8 μm) are generated by a two-stage optical parametric amplifier (OPA), based on a type II β-barium borate (BBO) crystal, used in combination with difference frequency mixing in a $AgGaS_2$ crystal. Generation of the mid-IR pulses follows closely the method described earlier by Hamm et al.[36] A small percentage of the mid-IR beam is reflected from the surface of a BaF_2 1° wedge to form the probe beam, which is then focused on the sample as described in detail elsewhere.[37] The probe beam is dispersed in a spectrograph (Acton Research Corp., $f = 150$ mm, 150 grooves/mm grating), and detected with one of the arrays of the 64 channel double array HgCdTe detector (Infrared Systems Development). The spectral resolution in the probed region was ∼2 cm^{-1}/pixel. The portion of the mid-IR beam that goes through the wedge is used as the pump. To disrupt the phase relationship between the probe and pump beams, the pump beam is reflected by a mirror mounted on a piezoelectric element after passing through a variable delay line. The piezoelectric element, driven at 50 Hz, has a maximum displacement of 9 μm at 150 V. Periodic displacement of the piezo element causes the phase difference between pump and probe to be different for each of the laser shots averaged. This phase scrambling effect reduces coherent effects on the measured signals, which can be otherwise much stronger than the signal originating from transient absorption. From the piezo-mounted mirror, the beam is directed by two gold mirrors into the cryostat. About 1/3 of the 1 in. diameter circular CaF_2 substrate where the matrix is deposited was cut out so that in the first forward pass the pump beam crosses the cryostat without interacting with the matrix. The pump beam is then focused back into the cryostat by a 50 mm focal length gold mirror and overlapped with the probe beam at the rare-gas matrix in a counter-propagating configuration. Every second pump pulse is blocked by a synchronized chopper; the transient signal is obtained by comparing the probe signal with and without mid-IR excitation. For all of the studied species, a broadband femtosecond pulse centered at 1739 cm^{-1} (fwhm ≈ 150 cm^{-1}) was used to excite the $\nu_{C=O}$ mode. Typically, 1000 shots were collected per data point, and 20 independent scans were averaged before analysis.

Results

Isolated Monomers. The steady-state spectra of FA and AA recorded by the femtosecond spectrometer and by the FTIR spectrometer for the 0.3−0.4% matrix samples are compared in Figure 1. The steady-state bands at 1767 cm^{-1} (FA in Figure 1a) and 1779 cm^{-1} (AA, in Figure 1b) observed in the nonirradiated argon matrices are the well-known $\nu_{C=O}$ bands of the lower energy conformer of the isolated monomer.[2] The minor bands at lower frequencies belong to the corresponding dimers. Contribution from the dimers to the spectra of these relatively low concentration samples is noticeably small and very well isolated from the monomer bands.

Typically, excitation of the $1 \leftarrow 0$ transition of a given vibrational mode results in a negative signal at the position of the $1 \leftarrow 0$ absorption with equal contributions from the bleaching of the vibrational ground-state population, and from the $0 \leftarrow 1$ stimulated emission.[33] In addition, a positive signal emerges

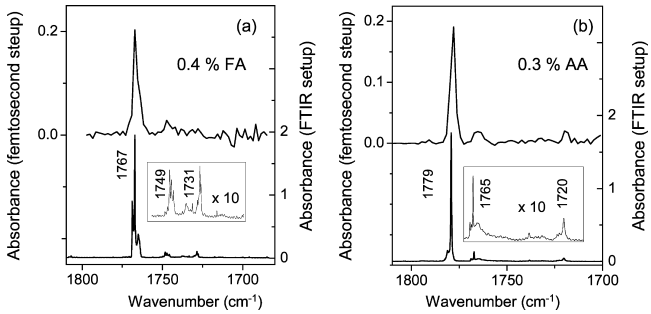

Figure 1. Steady-state spectra of FA and AA recorded by the femtosecond spectrometer (upper trace) and by conventional FTIR spectroscopy (lower trace) for the less concentrated mixtures of FA (a) and AA (b) in argon. The dimer bands are magnified in the inset. For each setup (femtosecond or FTIR), the spectra were measured in different matrices.

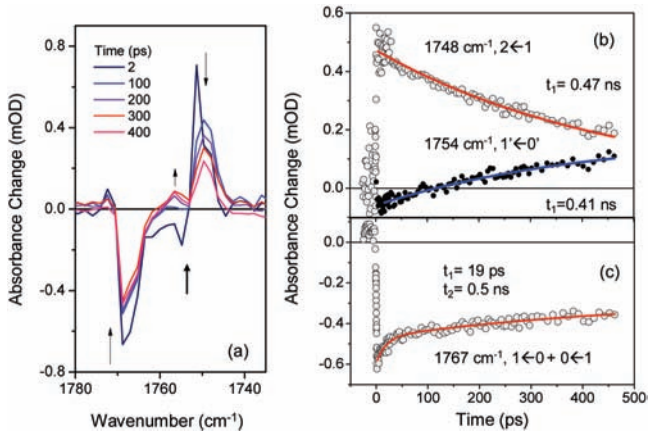

Figure 2. Transient spectrum of FA recorded at selected times after excitation with a broadband pulse centered at 1739 cm^{-1} (a), and kinetics of the relevant features in the transient spectra (b and c). In plots b and c, the experimental data points are represented by symbols, and the curves resulting from biexponential fits to these data points are shown as solid lines. The fitting parameters are shown in detail in Table 1.

from absorption of the excited state ($2 \leftarrow 1$ hot transition) red-shifted from the $1 \leftarrow 0$ transition due to anharmonicity.[33] Evolution of the initially excited-state population is reflected on both the excited-state absorption and the stimulated emission. Population transfer into other vibrational modes results in a perturbed fundamental absorption of the originally excited mode ($1' \leftarrow 0'$), which appears slightly shifted to higher or lower frequencies from the fully vibrationally relaxed ground state.[27,33]

For FA, temporal evolution of the transient spectrum is shown in Figure 2 together with the kinetics of the relevant transient features. The parameters of all of the kinetic fits discussed in this article are collected in Table 1. Excitation of the $1 \leftarrow 0$ transition of the $\nu_{C=O}$ mode induces a negative signal at 1767 cm^{-1} due to instantaneous bleaching of the ground state and stimulated emission. Simultaneously, absorption due to the $2 \leftarrow 1$ hot transition appears at 1748 cm^{-1}. The assignment of the band at 1748 cm^{-1} to the hot transition is supported by the previously reported values for the $2 \leftarrow 0$ and $1 \leftarrow 0$ transitions at 3519−3516 and 1769−1767 cm^{-1}, respectively.[16] At early times, a relatively weak negative transient is observed at 1754 cm^{-1}. Assignment of this signal to stimulated emission into a coupled phonon/libration state will be discussed later. At later times, a new absorption becomes evident at 1755 cm^{-1}, which is assigned to absorption from a perturbed ground state ($1' \leftarrow 0'$).

The temporal evolution of the transient spectrum of monomeric AA is shown in Figure 3, together with the kinetic traces of its relevant features. For AA, all of the dynamics is nearly completed within our temporal observation window of 360 ps. Except for the time scale, the vibrational energy relaxation dynamics following the $\nu_{C=O}$ excitation of AA is quite similar to that of the FA monomer. There are four relevant features in the transient spectra: the negative signal at 1779 cm^{-1} due to the ground-state bleach and $0 \leftarrow 1$ stimulated emission, the transient absorption band of the excited $\nu_{C=O}$ mode ($2 \leftarrow 1$) at 1762 cm^{-1}, and a delayed absorption band at 1774 cm^{-1}. The negative band at 1765 cm^{-1} shown in Figure 3a is assigned to stimulated emission into a coupled phonon/libration state, similarly to the FA band at 1755 cm^{-1}. The band has also a contribution of about 30% of its intensity from impurity FA.

Dimers. For FA, the dimer dynamics was probed in more concentrated matrices showing an enriched dimer population. The dimer conformers relevant to the present study are depicted in Figure 4. The steady-state spectra of a typical matrix sample used in the studies of the FA dimers are shown in the lower plot of Figure 5. The intense bands observed at 1749 and 1731 cm^{-1} are characteristics of the $\nu_{C=O}$ fundamental transition in the dimers.[14] The band at 1731 cm^{-1} is the signature of the centrosymmetric 8-membered ring dimer labeled CS in Figure 4. In the CS dimer, the two C═O bonds are involved in intramolecular hydrogen bonding. The higher energy open-chain dimer (OC) with one ═O···HO intermolecular bond and a free hydroxyl group gives rise to the band at 1749 cm^{-1}.

For FA, the upper plot in Figure 5 shows the transient spectra at different delay times. The transient spectra of the highly monomeric matrix were subtracted from the dimer enriched transient spectra to minimize the contribution from the monomer dynamics in the transient spectra shown in Figure 5. Because of a considerable band overlap between the OC dimer ground-state absorption (1749 cm^{-1}) and the monomer excited-state absorption (1748 cm^{-1}), subtraction of the monomer contribution is essential for a clear observation of the OC dimer dynamics. However, it should be noted that due to differences in the concentration and deposition conditions of the monomer-enriched and dimer-enriched matrices, the steady-state absorption of the monomer appears slightly red-shifted in the dimer-enriched matrix, causing an artifact on the monomer transients, which is evident at 1767 cm^{-1} in Figure 5. For the OC and CS dimers, the broadband excitation induces negative transients due to bleaching of the $v = 0$ population and stimulated emission from $v = 1$ at 1749 cm^{-1} (OC) and 1731 cm^{-1} (CS), respectively. The bands of the corresponding excited-state absorption ($2 \leftarrow 1$) appear shifted to the red from each of the negative dimer signals, at 1740 cm^{-1} (OC) and 1722 cm^{-1} (CS). The $1' \leftarrow 0'$ delayed absorption transients appear at 1745 cm^{-1} (OC) and 1727 cm^{-1} (CS). Coupling of the $\nu_{C=O}$ mode with the transiently excited modes leads to a 4 cm^{-1} red-shift with respect to the fundamental transition in a vibrationally relaxed molecule. The kinetics of the relevant transient bands discussed above are depicted in Figures 6 and 7 for the OC and CS dimers, respectively.

The results for the AA dimer were obtained in a matrix with concentration similar to that shown in Figure 1b where the monomer is the predominant form. For the CS dimer of AA, the transient spectra at different delay times are shown in Figure 8, together with the kinetics of the negative transient. Because of the low concentration of the CS dimer, it was not possible to follow the kinetics of the transient excited-state absorption.

TABLE 1: Time Constants (t, ps) and Amplitudes (A, mOD) Obtained in the Fitting of Exponential Decay Functions[a] to the Kinetics of the Transient Features Observed upon Broadband Excitation of the $\nu_{C=O}$ of the Monomer (M) and Dimer (CS and OC) of FA and AA

molecular species	bleach and stimulated emission $\nu_1 \leftarrow \nu_0$ and $\nu_0 \leftarrow \nu_1$	delayed absorption $\nu_{1'} \leftarrow \nu_{0'}$	hot transition $\nu_2 \leftarrow \nu_1$
FA-M	1767 cm^{-1} $t_1 = 19 \pm 3.5$, $A_1 = -0.11$ $t_2 = 512 \pm 47$, $A_2 = -0.19$ off set $= -0.27$	1754 cm^{-1} $T_1 = 412 \pm 93$, $A_1 = -0.23$	1748 cm^{-1} $t_1 = 467 \pm 14$, $A_1 = 0.47$
FA-CS	1731 cm^{-1} $t_1 = 10$ fixed, $A_1 = -1.3$ $t_2 = 39$ fixed, $A_2 = -0.4$ $t_3 = 515 \pm 55$, $A_3 = -1$	1727 cm^{-1} $t_1 = 10 \pm 2.5$, $A_1 = -0.4$ $t_2 = 79 \pm 17$, $A_2 = -1$ $t_3 = 489 \pm 71$, $A_3 = 1.2$	1722 cm^{-1} $t_1 = 10 \pm 3$, $A_1 = 1.5$ $t_2 = 39 \pm 8$, $A_2 = 1.3$
FA-OC[b]	1749 cm^{-1} $t_1 = 34 \pm 4$, $A_1 = -1.3$ $t_2 = 570 \pm 198$, $A_2 = -0.4$		1740 cm^{-1} $t_1 = 30 \pm 4$, $A_1 = 0.9$ $t_2 = 243 \pm 33$, $A_2 = 0.6$
AA-M[c]	1779 cm^{-1} $t_1 = 5 \pm 2$, $A_1 = -0.13$ $t_2 = 84 \pm 8$, $A_2 = -0.60$	1774 cm^{-1} $t_1 = 54 \pm 14$, $A_1 = -0.6$ $t_2 = 84$ fixed, $A_2 = 0.6$	1762 cm^{-1} $t_1 = 5 \pm 2$, $A_1 = 0.5$ $t_2 = 84 \pm 8$, $A_2 = 0.7$
AA-CS	1720 cm^{-1} $t_1 = 8 \pm 2$, $A_1 = -0.1$ $t_2 = 88 \pm 6$, $A_2 = -0.3$		

[a] $\Delta A = \sum_i A_i \exp[-(x - x_0)/t_i]$. [b] Overlapping of the FA-OC bands with the monomer excited-state absorption causes some indetermination on the time constant associated with its slower dynamics. [c] Results from a global fitting of the bleach/stimulated emission and hot transition signals.

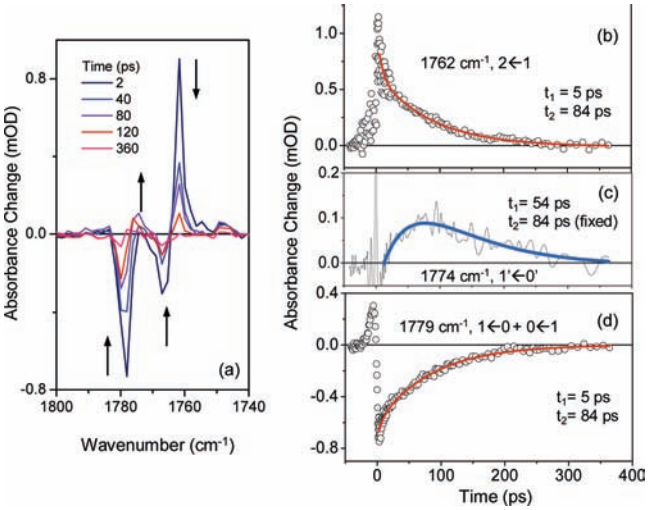

Figure 3. Transient spectrum of AA recorded at selected times after excitation with a broadband pulse centered at 1739 cm^{-1} (a), and kinetics of the relevant features in the transient spectra (b−d). In plots b, c, and d, the experimental data points are represented by symbols, and the curves resulting from biexponential fits to these data points are shown as solid lines. The fitting parameters are shown in detail in Table 1.

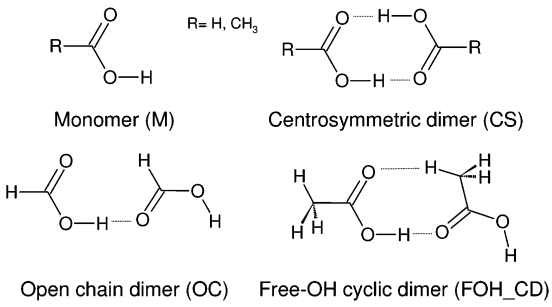

Figure 4. Structure of the monomeric and dimeric units of FA and AA.

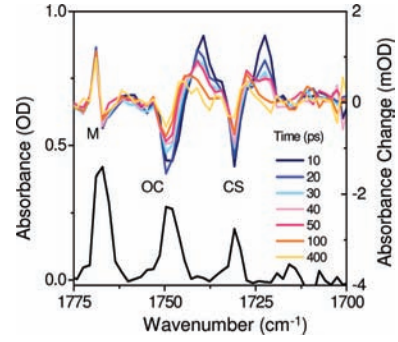

Figure 5. Transient spectra at different delay times (upper trace) and steady-state spectra collected by the array detector in the matrix with lower monomer/dimer ratio used to study the dimer dynamics (lower trace). The labels M, OC, and CS stand for monomer, open chain, and centrosymmetric dimer, according to Figure 4.

Discussion

Monomer Dynamics. For FA, evolution of the 2 ← 1 band at 1748 cm^{-1} reflects exclusively the population of the $v = 1$ state. Hence, it allows separation of the contribution of 0 ← 1 stimulated emission to the negative signal at 1767 cm^{-1} from the contribution of the bleaching of the $v = 0$ population. As shown in Figure 2b, the 2 ← 1 band decays with a time constant of ∼470 ps. Nearly 60% of this transient absorption decays within the 450 ps window of observation. Hence, the decay of the negative signal by 38% within 450 ps (see Figure 2c) corresponds essentially to the expected decay of the contribution from stimulated emission (the band intensity is expected to decay by 1/2 × 60% = 30% due to stimulated emission, because in a harmonic approximation the intensity of the 2 ← 1 transition is twice the intensity of the 0 ← 1 transition). Thus, the temporal observation window of 450 ps is too narrow to resolve the contribution of recovery of the ground-state population to the kinetics of the negative transient. The recovery time is estimated to be in the nanosecond regime (≥5 ns). This value is consistent with the existence of large energy gaps in the vibrational manifold of FA. The lowest energy vibrational modes of FA (OCO bending and C−O torsion) have vibrational frequencies of ∼630 cm^{-1}.[16] For comparison, for HONO a clear cascading of the excitation energy through the ONO bending mode (vibrational quanta of ∼600 cm^{-1}) leads to a 20 ns relaxation process.[34]

Apart from the slow decay component, a fast decay with a time constant of 19 ps is observed in the kinetics of the negative transient. This fast decay is also assigned to the decay of stimulated emission, despite the fact that it is not readily observed in the decay of the excited-state absorption. Instead, the transient absorption shows oscillatory behavior at early times that obscures the fast time component. The origin of these oscillations is not clear at the moment. The fast decay component (19 ps) accounts for ∼37% of the decay of the stimulated emission signal. In this context, it is worth mentioning that FA is distributed in the matrix in two main sites with a relative population of 38%:62%.[16] Given the similarity between the site distribution and the relative contribution of the fast and slow relaxation channels, it is possible that the biexponential kinetics is due to different sites having different kinetics. On

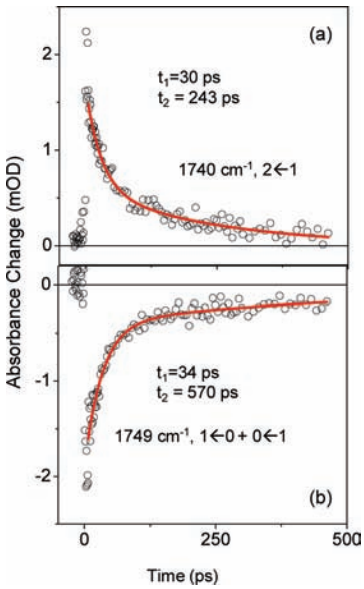

Figure 6. Kinetics of the transient features associated with excitation of the $\nu_{C=O}$ of the OC dimer of FA: (a) decay of the excited-state absorption of the $\nu_{C=O}$ mode at 1740 cm^{-1}, and (b) recovery of the negative transient at 1749 cm^{-1}. The experimental data points are represented by symbols, and the curves resulting from biexponential fits to these data points are shown as solid lines. Note that the negative transient overlaps the monomer excited-state absorption, and thus the long time constant is affected by a significant experimental error (see Table 1).

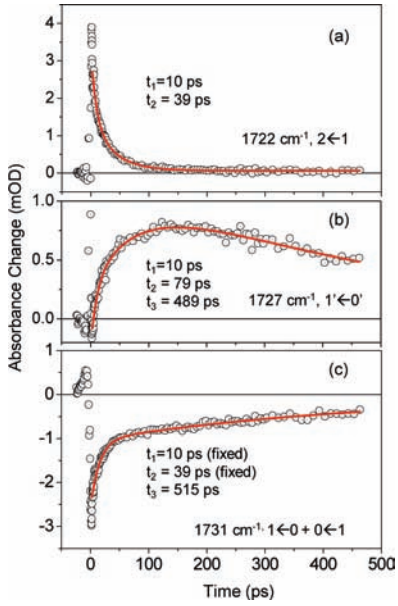

Figure 7. Kinetics of the transient features associated with excitation of the $\nu_{C=O}$ of the CS dimer of FA: (a) decay of the initially excited-state absorption at 1722 cm^{-1}, (b) kinetics of fundamental $\nu_{C=O}$ transition in the hot molecule (1727 cm^{-1}) reflecting the population of the intermediate excited state, and (c) recovery of the bleach and stimulated emission signal overlapping at 1731 cm^{-1}. The fitting parameters are collected in Table 1.

the other hand, the small splitting induced by the matrix site distribution on the vibrational transitions (<3 cm^{-1}) is not compatible with large difference in kinetics.

The fact that the bleach of the ground-state population does not recover significantly within 450 ps, while the population of the $\upsilon = 1$ state decays by 60%, indicates that the excitation is transferred to intermediate vibrational modes. The weak delayed absorption at 1754 cm^{-1} is a signature of such a process. This

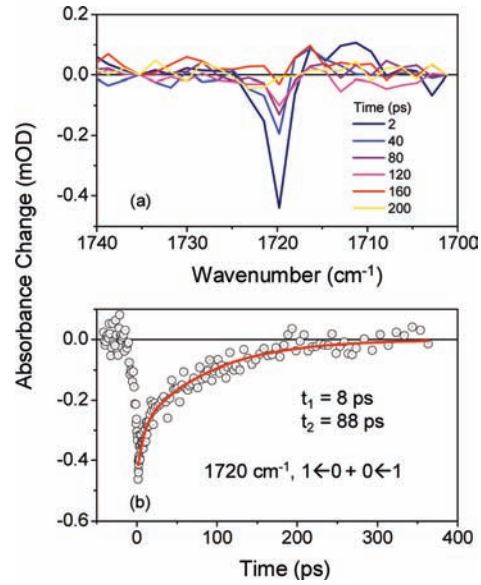

Figure 8. Evolution of the transient $\nu_{C=O}$ bleach of the CS dimer of AA: (a) transient spectra recorded at different times, and (b) kinetics followed at 1720 cm^{-1}. In trace (b), the experimental data points are represented by symbols, and the curve resulting from a biexponential fit to these data points is shown as a solid line. The fitting parameters are shown in detail in Table 1.

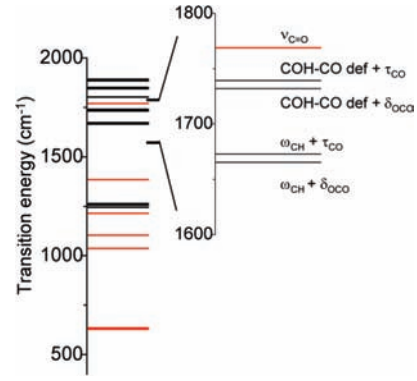

Figure 9. Vibrational state distribution estimated from the measured transitions in the Ar matrix including known anharmonicity data.[16,38] The symbols stand for: def, deformation; τ, torsion; δ, angular deformation; ω, wagging.

band is assigned to the $1' \leftarrow 0'$ transition of the $\nu_{C=O}$ mode in a molecule in which other vibrational modes are excited. In this hot state, the anharmonic couplings between the $\nu_{C=O}$ mode and the bath of excited modes shift the $\nu_{C=O}$ fundamental transition to the red by 12 cm^{-1}. The magnitude of this shift depends linearly on the anharmonic coupling constants, and on the level of excitation of the coupled modes.[34] The $1' \leftarrow 0'$ delayed absorption grows with a time constant (~410 ps) nearly equal to that of the decay of the $\upsilon = 1$ population (~470 ps).

Identification of the specific relaxation pathways is not a trivial task even for FA, which, at this excitation level, has a very low density of vibrational states. The distribution of the vibrational states, estimated from the measured transitions in the Ar matrix including the known anharmonicity data,[16,38] is represented in Figure 9. Four combination modes are expected to lie within less than 200 cm^{-1} below the $\upsilon = 1$ state of the $\nu_{C=O}$. Two of these modes have A′ symmetry like the initially excited mode, the COH−CO def + δ_{OCO} and the ω_{CH} + τ_{CO} (the symbols stand for: def, deformation; τ, torsion; δ, angular deformation; ω, wagging). These modes lay within a one-phonon transition from each other, and thus they are good

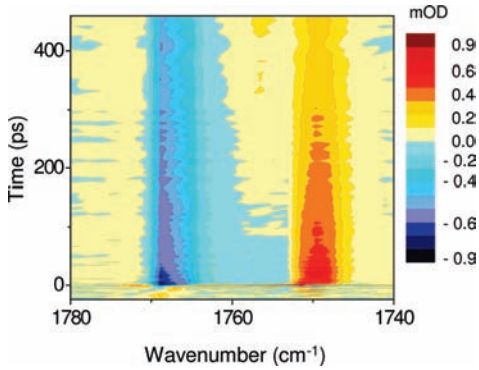

Figure 10. Contour plot showing a broad and weak negative feature appearing at early times between the ground-state bleach (1767 cm^{-1}) and the excited-state absorption band (1749 cm^{-1}). The delayed absorption of the intermediately excited state appears at later times at 1754 cm^{-1}.

candidates to the first tier of intermediate states accepting energy from the $\nu_{C=O}$ mode. The two possible accepting modes involve one quantum of either the δ_{OCO} or the τ_{CO}, which have the two lowest energy quanta in FA. Nearly 300 cm^{-1} separates this first group of vibrational states from the second cluster of states found in the 1400−1000 cm^{-1} region. A higher order phonon excitation is needed to compensate for this energy mismatch, creating a bottleneck that can partially explain the slow ground-state recovery.

It is worth noting a weak negative transient red-shifted from the strong bleach signal (extending all of the way from the bleach to the hot absorption signals), which is particularly evident at early times (see Figure 10). A possible explanation for this broad negative signal red-shifted from the ground-state absorption is stimulated emission from the initially excited vibrational state into a coupled libration/phonon excited state resulting from the coupling of the molecular librational motion or lattice vibrational modes with the ground state of the $\nu_{C=O}$ mode. Indeed, the coupling of the intramolecular vibrations with the librational and phonon modes produces sidebands blue-shifted from the pure intramolecular transition.[39] The phonon−vibration coupling is too weak to lead to an appreciable sharing of oscillator strength, thus making it difficult to observe the phonon sideband in the absorption spectra, but it is sufficiently strong to be observed in the more sensitive reactive-excitation spectra.[39] On the other hand, a sideband assigned to the vibration + libration mode is readily observable in the absorption spectrum.[39] In the present case, we assign the red-shifted negative sideband to stimulated emission from the initially excited state to the vibrational ground state with simultaneous excitation of a libration/phonon mode.

For AA, both the decay of the negative signal at 1779 cm^{-1} and the decay of the excited-state population determined at 1762 cm^{-1} are well fitted by a biexponential kinetics with a fast decay of ∼5 ps and a slower dominant decay of ∼84 ps (see Figure 3 and Table 1). Again, the presence of a weak delayed absorption at 1774 cm^{-1} shows that the excess energy originally deposited in the $\nu_{C=O}$ mode is first transferred into intramolecular bath modes, and later relaxed into the host phonon modes. Population of the intermediate states follows a time constant (54 ps in Figure 3c) similar to the depopulation of the initially excited state (84 ps in Figure 3). Given the low intensity of the delayed absorption transient and its partial overlap with the negative transient, this small difference in decay constants can be attributed to experimental inaccuracy. As shown in Figure 3c, the depopulation of the intermediately excited states is perfectly described by a time constant matching that of the recovery of the bleach (84 ps).

As for FA, the site splitting is a possible reason for the biexponential kinetics observed in the excited-state decay and bleach recovery of AA. However, the splitting in the FTIR absorption spectra of AA is not so evident as in FA.[17] Thus, the origin of the biexponential kinetics observed for both molecules remains unclear. As it will be discussed later, the dimer dynamics shows also a biexponential population transfer process for both FA and AA. It is worth noting that a biexponential kinetics was also reported earlier for the AA dimer in CCl_4 solutions and thought to be connected with environmental effects.[31]

Regardless of the origin of the biexponential population transfer, for the AA monomer, both the redistribution of population into intermediate intramolecular states and the energy dissipation into the lattice modes have similar time scales. In AA, as compared to FA, the population transfer from the initially excited $\nu_{C=O}$ into the intermediate states is faster by a factor of 5, and energy dissipation into the lattice is more than 1 order of magnitude faster. These differences may be ascribed to the participation of the methyl group in the relaxation process. They reflect the increased density of intramolecular states (∼0.3 states/cm^{-1} at energies corresponding to excitation of one quantum of the $\nu_{C=O}$) due to the low energy quanta of the methyl torsion (τ_{CH3}), which was estimated to be 60−80 cm^{-1} by ab initio methods.[17] The increased rate of population transfer from the initially excited mode in AA suggests the methyl group to be well coupled to the $\nu_{C=O}$ mode. On the other hand, the increased energy dissipation into the host shows that these modes are also well coupled to the lattice phonons.

The important participation of the methyl group in the relaxation dynamics is most probably the explanation for the 1 order of magnitude lower quantum yield for trans → cis conformational isomerization for AA as compared to FA.[39,40] The difference in the isomerization quantum yield is a consequence of a less efficient energy transfer to the reaction coordinate (intimately connected with the τ_{CO} mode) in AA as a result of competing nonreactive energy relaxation channels associated with the methyl group.

Dimer Dynamics. For the CS dimer of FA, absorption from the initially excited state shows a fast biexponential decay with associated time constants of ∼10 and 39 ps (see Figure 7a and Table 1). The delayed absorption at 1727 cm^{-1} exhibits also a relatively fast growth (fitted with a biexponential function with time constants of 10 and 79 ps in Figure 7b), albeit somewhat slower than the decay of the 2 ← 1 transition. Note that the delayed absorption overlaps with the ground-state bleach, and thus the time constants associated with the delayed absorption should not be taken too literally. As inferred from the decay of the delayed absorption (Figure 7b), relaxation of these intermediate states has a time constant of ∼500 ps.

The contribution from stimulated emission to the kinetics of the negative CS dimer band at 1731 cm^{-1} is expected to be a biexponential decay with the time constants characteristic of the transfer of the excited-state population (10 and 39 ps) into intermediate states. In addition, a much slower decay due to recovery of the bleached ground-state population is expected with the time constant matching the decay of the delayed absorption band (∼500 ps). Indeed, fitting the kinetics of the negative signal of the CS dimer by a three-exponential decay, with two fixed time constants associated with stimulated emission, results in a third longer time constant of ∼500 ps, in

good agreement with the decay of the intermediate state population (see Figure 7c and fitting parameters in Table 1).

For the OC dimer of FA, both the relaxation of the initially excited state (probed at 1740 cm^{-1}) and the overall cooling of all of the vibrational degrees of freedom (followed by the recovery of the negative signal at 1749 cm^{-1}) follow a similar kinetics described by a dominant shorter time constant of ~30 ps and a longer time constant of 200−600 ps. The origin of the longer time component in the decay of the band at 1740 cm^{-1} is associated with the decay of the intermediately excited states, whose broad absorption band overlaps considerably with the initial excited-state absorption (see Figure 5).

The dynamics of the two dimers appears to be quite similar in that both have vibrational cooling times about 1 order of magnitude longer than the initially excited-state lifetime. This observation is somewhat unexpected in that the different symmetry of the two dimer conformers is expected to affect the vibrational dynamics. The CS dimer is a highly symmetric structure; it belongs to the C_{2h} symmetry group. Only 9 of its 24 fundamental modes of vibration belong to the same symmetry of the initially excited $\nu_{C=O}$ mode (B_u symmetry).[41] On the other hand, the OC dimer belongs to the C_s symmetry group, with 21 fundamental modes of vibration that belong to the same symmetry species of the excited $\nu_{C=O}$ mode (A′). Therefore, a higher density of vibrational modes with the appropriate symmetry could, in principle, lead to a faster dynamics in the OC dimer. On the other hand, H-bonding is expected to accelerate vibrational relaxation in the CS dimer. Note that the nature of the excited $\nu_{C=O}$ in the two dimers is fundamentally different. For the OC dimer the excited mode is the free C═O bond stretching, while for the CS dimer the excited C═O bond is involved in an intermolecular hydrogen bond. A more efficient coupling of the bonded $\nu_{C=O}$ mode in the CS dimer with the intermolecular ring modes is likely to lead to a faster dynamics in the CS dimer. Indeed, the observed similarities in the dynamics of the two dimers could be due to a compensation of effects (symmetry and H-bonding) acting in opposing directions. Despite the estimated barrier of only 700 cm^{-1} for the OC → CS isomerization, excitation of the $\nu_{C=O}$ of the CS dimer turned out to be unable to induce isomerization at 15 K. The confinement exerted by the solid environment hinders the rotation of the monomer unit around the ═O···OH bond during the lifetime of the excited state.

For FA, relaxation of the initially excited-state population is an order of magnitude slower in the monomer (~470 ps) than in the dimer (10−40 ps). The energy transfer to the host is also at least 1 order of magnitude slower for the FA monomer (estimated as ≥5 ns) as compared to the dimers (~500 ps). Similarly to the methyl rotor effect on the dynamics of the monomers, these observations are consistent with the increased density of vibrational states in the dimers, connected with the low energy quanta (68−248 cm^{-1})[41] of the intermolecular modes.

For the AA dimer, the kinetics of the negative transient can be fitted with a biexponential decay with time constants of ~8 and ~88 ps (see Figure 8b and Table 1). Contrary to FA, the vibrational cooling rates have similar time constants for the monomer and the CS dimer of AA. This similarity indicates that the role of the methyl group in mediating the energy transfer into the solvent bath is at least as relevant in the monomer as that of the intermolecular ring modes in the dimer. On the other hand, the vibrational cooling rate for the CS dimer is clearly faster in AA (factor of ~5) than in FA, showing that the methyl group has an important role in the energy dissipation process also in the dimer.

In early single color pump and probe studies on the vibrational dynamics induced by excitation of the ν_{OH} in the FA and trifluoroacetic acid CS dimers, both in the gas phase and in solution, it was concluded that vibrational relaxation has no significant contribution from nonring modes, based on the similarity between the dynamics of the two dimers. Indeed, as mentioned in the Introduction, FA, AA, propionic acid, and benzoic acid dimers in solution display a very similar vibrational dynamics upon excitation of the ν_{OH} mode. From the data presented here, it is evident that the $\nu_{C=O}$, unlike the ν_{OH}, is relatively decoupled from the ring modes, which is somewhat surprising. In addition, the weakly interacting environment and the low temperatures lead to much slower dynamics than in solution. Recovery of the overall ground-state population upon excitation of the $\nu_{C=O}$ of AA in solution at room temperature (~8 ps)[31] is 1 order of magnitude faster than in the low temperature matrix (~88 ps). The slower vibrational cooling in the rare-gas matrix can certainly be understood as an effect of the reduced spectral overlap between the guest molecule and the host matrix, and the fact that in conventional solvents the intramolecular modes, translational, and rotational degrees of freedom of the solvent can all participate as accepting modes.

Conclusions

The vibrational dynamics of AA and FA isolated in an Ar matrix was investigated by ultrafast IR spectroscopy. The results can be summarized as follows:

(i) For the monomer, depopulation of the initially excited state of AA is by a factor of 7 faster than in FA, showing that the methyl group has a relevant participation in the dynamics of intramolecular energy redistribution.

(ii) The faster vibrational energy transfer to the environment in AA (monomer and CS dimer) as compared to FA is clear evidence of participation of the methyl group also in the dynamics of vibrational cooling.

(iii) Hydrogen bonding speeds up the vibrational dynamics in the FA dimers. This effect is evidenced by 1 order of magnitude faster depopulation of the initially excited state, and a faster energy relaxation into the lattice phonons in the FA dimers as opposed to the monomer.

(iv) However, for AA, hydrogen bonding has apparently no effect on the vibrational cooling rate. Both monomer and dimer have similar relaxation kinetics, suggesting that the methyl rotor is more relevant to the relaxation dynamics than are the ring modes.

Some observations remain unclear, like the origin of the biexponential dynamics observed for both monomers and dimers. As a future development of the present work, refinement of the data on the AA dimer dynamics and investigation of dynamics upon excitation of different vibrational modes are planned.

Acknowledgment. E.M.S.M. acknowledges financial support from a Marie-Curie fellowship (contract no.: 023586), an exchange grant of the European Science Foundation (DYNA programme, grant 2000), and an FCT grant (ref SFRH/BD/38601/2007).

References and Notes

(1) Pettersson, M.; Maçôas, E. M. S.; Khriachtchev, L.; Fausto, R.; Räsänen, M. *J. Am. Chem. Soc.* **2003**, *125*, 4058.

(2) Maçôas, E. M. S.; Khriachtchev, L.; Pettersson, M.; Lundell, J.; Fausto, R.; Räsänen, M. *Vib. Spectrosc.* **2004**, *34*, 73.

(3) Marushkevich, K.; Khriachtchev, L.; Räsänen, M. *Phys. Chem. Chem. Phys.* **2007**, *9*, 5748.
(4) Marushkevich, K.; Khriachtchev, L.; Räsänen, M. *J. Chem. Phys.* **2007**, *126*, 241102.
(5) Pettersson, M.; Maçôas, E. M. S.; Khriachtchev, L.; Lundell, J.; Fausto, R.; Räsänen, M. *J. Chem. Phys.* **2002**, *117*, 9095.
(6) Marushkevich, K.; Khriachtchev, L.; Räsänen, M. *J. Phys. Chem. A* **2007**, *111*, 2040.
(7) Gantenberg, M.; Halupka, M.; Sander, W. *Chem.-Eur. J.* **2000**, *6*, 1865.
(8) Sanchez-Garcia, E.; Studentkowski, M.; Montero, L. A.; Sander, W. *ChemPhysChem* **2005**, *6*, 618.
(9) Ortlieb, M.; Havenith, M. *J. Phys. Chem. A* **2007**, *111*, 7355.
(10) Mil'nikov, G.; Kuhn, O.; Nakamura, H. *J. Chem. Phys.* **2005**, 1123.
(11) Barnes, G. L.; Squires, S. M.; Sibert, E. L. *J. Phys. Chem. B* **2008**, *112*, 595.
(12) Madeja, F.; Havenith, M. *J. Chem. Phys.* **2002**, *117*, 7162.
(13) Turi, L.; Dannenberg, J. J. *J. Phys. Chem.* **1993**, *97*, 12197.
(14) Sander, W.; Gantenberg, M. *Spectrochim. Acta, Part A: Mol. Biomol. Spectrosc.* **2005**, *62*, 902.
(15) Halupka, M.; Sander, W. *Spectrochim. Acta, Part A: Mol. Biomol. Spectrosc.* **1998**, *54*, 495.
(16) Maçôas, E. M. S.; Lundell, J.; Pettersson, M.; Khriachtchev, L.; Fausto, R.; Räsänen, M. *J. Mol. Spectrosc.* **2003**, *219*, 70.
(17) Maçôas, E. M. S.; Khriachtchev, L.; Fausto, R.; Räsänen, M. *J. Phys. Chem. A* **2004**, *108*, 3380.
(18) Khriachtchev, L.; Maçôas, E.; Pettersson, M.; Räsänen, M. *J. Am. Chem. Soc.* **2002**, *124*, 10994.
(19) Marushkevich, K.; Khriachtchev, L.; Lundell, J.; Räsänen, M. *J. Am. Chem. Soc.* **2006**, *128*, 12060.
(20) Matylitsky, V. V.; Riehn, C.; Gelin, M. F.; Brutschy, B. *J. Chem. Phys.* **2003**, *119*, 10553.
(21) Riehn, C.; Matylitsky, V. V.; Gelin, M. F.; Brutschy, B. *Mol. Phys.* **2005**, *103*, 1615.
(22) Shipman, S. T.; Douglass, P. C.; Yoo, H. S.; Hinkle, C. E.; Mierzejewski, E. L.; Pate, B. H. *Phys. Chem. Chem. Phys.* **2007**, *9*, 4572.
(23) Seifert, G.; Patzlaff, T.; Graener, H. *Chem. Phys. Lett.* **2001**, *333*, 248.
(24) Heyne, K.; Huse, N.; Nibbering, E. T. J.; Elsaesser, T. *Chem. Phys. Lett.* **2003**, *369*, 591.
(25) Heyne, K.; Huse, N.; Nibbering, E. T. J.; Elsaesser, T. *Chem. Phys. Lett.* **2003**, *382*, 19.
(26) Heyne, K.; Huse, N.; Dreyer, J.; Nibbering, E. T. J.; Elsaesser, T.; Mukamel, S. *J. Chem. Phys.* **2004**, *121*, 902.
(27) Nibbering, E. T. J.; Elsaesser, T. *Chem. Rev.* **2004**, *104*, 1887.
(28) Yamaguchi, S.; Banno, M.; Ohta, K.; Tominaga, K.; Hayashi, T. *Chem. Phys. Lett.* **2008**, *462*, 238.
(29) Koller, F. O.; Huber, M.; Schrader, T. E.; Schreier, W. J.; Zinth, W. *Chem. Phys.* **2007**, *341*, 200.
(30) Banno, M.; Ohta, K.; Tominaga, K. *J. Phys. Chem. A* **2008**, *112*, 4170.
(31) Lim, M.; Hochstrasser, R. M. *J. Chem. Phys.* **2001**, *115*, 7629.
(32) Hamm, P. *Chem. Phys.* **2008**, *347*, 503.
(33) Schanz, R.; Botan, V.; Hamm, P. *J. Chem. Phys.* **2005**, *122*, 044509.
(34) Botan, V.; Schanz, R.; Hamm, P. *J. Chem. Phys.* **2006**, *124*, 234511.
(35) Apkarian, V. A.; Weitz, E. *J. Chem. Phys.* **1982**, *76*, 5796.
(36) Hamm, P.; Kaindl, R. A.; Stenger, J. *Opt. Lett.* **2000**, *25*, 1798.
(37) Maçôas, E. M. S.; Kananavicius, R.; Myllyperkiö, P.; Pettersson, M.; Kunttu, H. *J. Phys. Chem. A* **2007**, *111*, 2054.
(38) Freytes, M.; Hurtmans, D.; Kassi, S.; Lievin, J.; Auwera, J. V.; Campargue, A.; Herman, M. *Chem. Phys.* **2002**, *283*, 47.
(39) Maçôas, E. M. S.; Khriachtchev, L.; Pettersson, M.; Juselius, J.; Fausto, R.; Räsänen, M. *J. Chem. Phys.* **2003**, *119*, 11765.
(40) Maçôas, E. M. S.; Khriachtchev, L.; Pettersson, M.; Fausto, R.; Räsänen, M. *J. Chem. Phys.* **2004**, *121*, 1331.
(41) Brinkmann, N. R.; Tschumper, G. S.; Yan, G.; Schaefer, H. F. *J. Phys. Chem. A* **2003**, *107*, 10208.

JP8099384